CrossMark

Weldability of wrought Haynes® 282® repair welded using manual gas tungsten arc welding

Fabian Hanning[1] (iD) · Joel Andersson[2]

Abstract The ability of the precipitation hardening superalloy Haynes® 282® to be repaired by multi-pass gas tungsten arc welding is investigated in this study. The repair welding has been carried out on forged discs having four pre weld heat treatments, resulting in different grain sizes and precipitate structures of the base material. Another set of discs has additionally been put through a post weld heat treatment. The tendency to form cracks in the heat-affected zone and the fusion zone has been investigated metallographically. No cracks in the base metal heat-affected zone were found, whereas solidification cracks were present in the weld fusion zone of all tested conditions. While high heat input during welding increased cracking by a factor of 1.5, none of the heat treatments had a measurable influence on the cracking behaviour. Voids with solid state crack-like appearance turned out to be aluminium-rich oxides being present from the deposition of previous weld deposit layers.

✉ Fabian Hanning
fabian.hanning@chalmers.se

Joel Andersson
joel.andersson@hv.se

[1] Department of Industrial and Materials Science, Chalmers University of Technology, 412 96 Gothenburg, Sweden

[2] Department of Engineering Science, University West, Gustava Melins gata 2, 461 32 Trollhättan, Sweden

1 Introduction

Nickel-based superalloys are extensively used in hot sections of aircraft engines due to their high strength and creep resistance, with Alloy 718 being the standard grade for such applications for many years [1, 2]. The ongoing trend to increase engine efficiency, which is usually achieved by higher combustion temperatures, however requires development of new alloys which can be used in this more severe environment. One of the more recently developed alloys is Haynes® 282®, a γ′ hardening nickel-based superalloy having a maximum service temperature of ~ 800 °C [3].

Large structural components are often produced out of smaller parts that are later joined together by welding [4]. As the complex microstructure of superalloys makes them prone to crack formation, a profound understanding of the material behaviour and underlying mechanisms is necessary. This also holds for repair welding operations, which are, despite their complexity and difficulty, economically more feasible than replacing large components. The unique setup of such operations makes it difficult to develop automated (and thereby more controlled) methods, resulting in high responsibility resting on the shoulders of welders that carry out welding repairs. Nevertheless, the knowledge and understanding of ongoing mechanisms on the material side is paramount to be able to successfully use repair welding operations.

For Haynes® 282®, heat-affected zone (HAZ) cracking has been reported to occur by grain boundary liquation [5], with observations made during Gleeble hot ductility tests confirming the presence of liquid films at grain boundaries at high temperatures [6]. Material rankings using the constant heating rate test indicate a high resistance of Haynes® 282® to strain age cracking (SAC) [7, 8] and no cracking was found during post weld heat treatment (PWHT) in Haynes® 282® using autogenous laser welds [9]. The availability of studies on the welding

🖄 Springer

response of Haynes® 282® is however still very sparse and no information on multi-pass repair welding is available for this alloy yet. This study aims to fill this gap by investigating the influence of different pre and post weld heat treatments on HAZ and fusion zone (FZ) cracking during manual multi-pass repair welding. Furthermore, the effect of the welding process has been evaluated by varying the heat input through adjusting the welding current.

2 Experimental

2.1 Material and heat treatments

Wrought Haynes® 282® in the form of a 100-mm-diameter forged bar has been used for this study, with the nominal chemical composition given in Table 1. The as-received, solutionised condition had a grain size of ASTM 5.5 (51 ± 7 μm) and a hardness of 315 ± 7 HV with the microstructure showing strings of primary carbides typical for the thermomechanical history of the material (cf. Fig. 1a). Grain boundary carbides were not present in this material condition.

In total, eight discs with a thickness of 15 mm were cut from the bar and subsequently heat treated in a vacuum furnace with a heating rate of 4–11 °C/min and argon forced convection cooling down to 500 °C to minimise precipitation (cooling rate > 50 °C/min). The parameters are summarised in Table 2. Four heat treatment conditions have been selected to investigate the influence of pre weld material condition on weld cracking during repair welding. While the heat treatment at 1010 °C was chosen to just above the dissolution temperature of the γ′ phase in the material (997 °C [3]) without dissolving secondary carbides, the treatment at 1120 °C was selected to obtain a carbide distribution similar to the one obtained by using the recommended solutionising parameters. This temperature is the lower limit of the solution annealing window, which results in the removal of $M_{23}C_6$ carbides (1019 °C) from the grain boundaries, while M_6C and MC carbides remain in the material [3, 10]. The highest temperature was used to produce a coarse-grained material. The temperature represents the upper limit of the solution annealing window and together with the longer exposure time of 2 h (cf. 0.5 h for 1120 °C), an increase in grain size could be expected. Fully age hardened material has been reported to be more susceptible to weld cracking especially when it comes to SAC due to the localisation of strain to the HAZ [11]. One disc

has hence been put through a complete age hardening cycle (788 °C for 8 h) before being repair welded. Another four discs have been put through a post weld heat treatment after completing the repair welding operation. Direct ageing has been chosen opposed to the conventionally applied heating to solution treatment temperature to subject the material to more severe conditions. The reasoning here was that direct ageing results in a longer exposure time in the precipitation temperature range without heating to solution annealing temperature, where most of the stress relaxation occurs.

2.2 Repair welding

Five circular repair welding grooves with a diameter of 25 mm, a depth of 10 mm, and a bottom radius of 5 mm have been machined into the discs after the pre weld heat treatments, as indicated in Fig. 2a. To maximise welding restraint, the discs were fixed to 25-mm-thick stainless steel discs by a circumferential weld (cf. Fig. 2b). Repair welding has been carried out by experienced welders using manual gas tungsten arc welding (GTAW) with a tungsten-2% thorium (WT-20) electrode. Argon was used as shielding gas, with a nozzle gas flow of 8–15 l/min. Filler material in the form of 1.14-mm wire with matching chemistry has been used to fill the grooves. Two out of the five grooves have been filled using negative polarity and a welding current of 120 A, while 140 A have been used for the remaining ones. The former is typical for such a repair operation, whereas the higher weld current represents tougher conditions due to the higher heat input. The grooves have been filled with 7 to 8 layers, while the material was quenched by argon after the deposition of each layer to an inter-pass temperature of approximately 50 °C. The grooves have been filled one by one, but without specific sequence and no brushing between layer deposition.

2.3 Weld examination and microstructural analysis

Three cross sections have been cut out of each welded groove by abrasive waterjet cutting and subsequently mounted in hot mounting resin for automated metallographic preparation. Cross section positioning was transverse to the welding direction. One cross section was cut out from the centre line, while the remaining two were positioned parallel to the centre position with a distance of approximately 5 mm. Since the discs were cut off from a forged bar, the cross sections taken for weld examination show the base material in longitudinal direction. The cross sections were subsequently visually inspected for cracks and other imperfections by scanning over the polished surface at ×200 magnification using an Olympus BX60M light optical microscope. The relative position of found imperfections was recorded and images taken. For better identification, the samples were then electrolytically etched with 10 wt% oxalic acid at 3 V DC for 3–5 s, followed by re-inspecting the

Table 1 Nominal chemical composition in weight percentage of Haynes® 282®

Ni	Cr	Co	Mo	Ti	Al	Fe	Mn	Si	C	B
Bal	20	10	8.5	2.1	1.5	0.15[a]	0.3[a]	0.15[a]	0.06	0.005

[a] Max
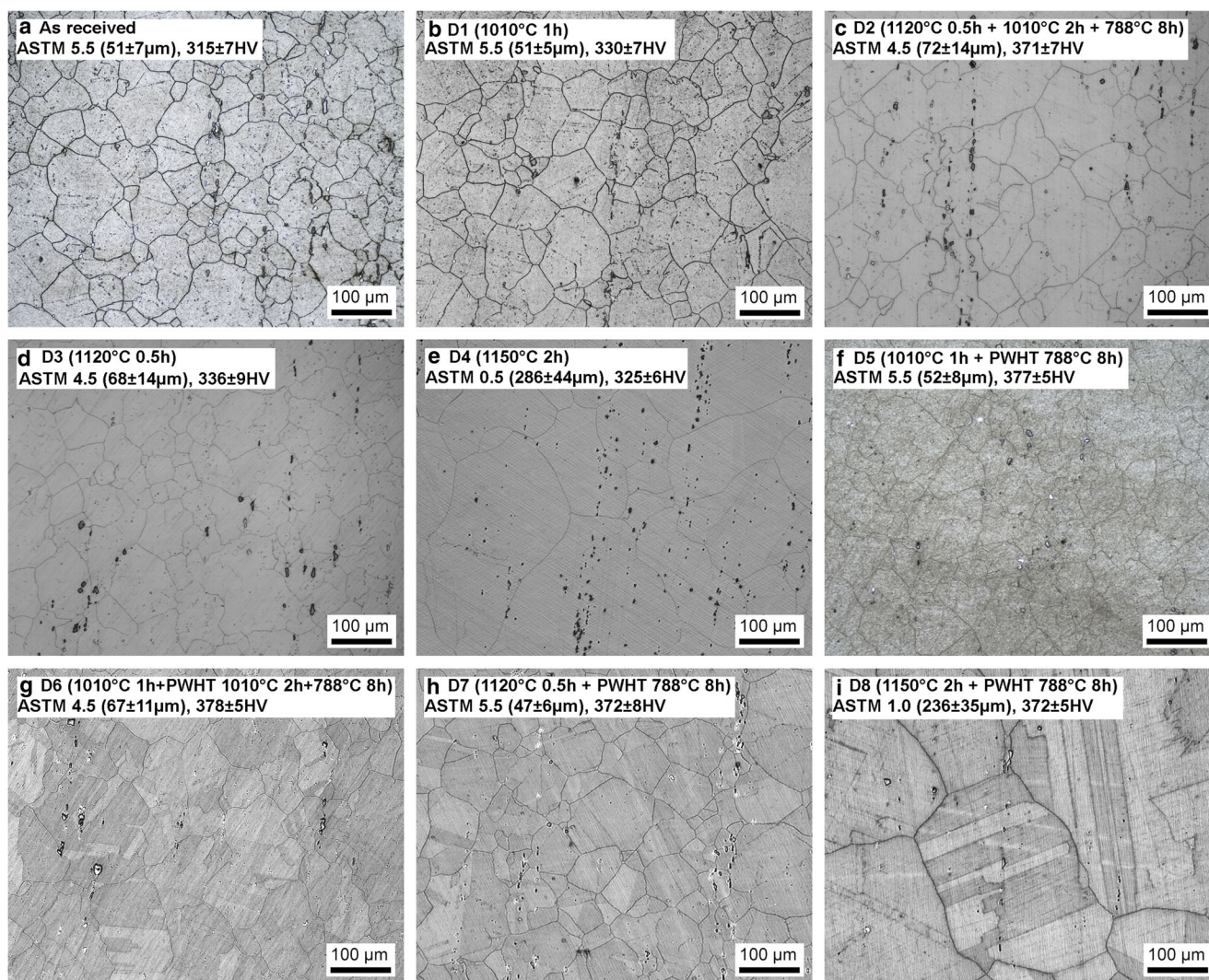
Fig. 1 Microstructure of the base material after different heat treatments, including respective grain size and hardness values

previously recorded imperfections. Imperfections were classified as either cracks, pores or lack of fusion (LoF) based on their appearance. A criterion for the latter was the smooth and curved shape and their sheer size.

Table 2 Pre and post weld heat treatment conditions

| Disc no.	Pre weld heat treatment	Post weld heat treatment
1	1010 °C—1 h	–
2	1120 °C—0.5 h + 1010 °C—2 h + 788 °C—8 h	–
3	1120 °C—0.5 h	–
4	1150 °C—2 h	–
5	1010 °C—1 h	788 °C—8 h
6	1010 °C—1 h	1010 °C—2 h + 788 °C—8 h
7	1120 °C—0.5 h	788 °C—8 h
8	1150 °C—2 h	788 °C—8 h

Microhardness has been measured on representative samples with a force of 0.5 kgf (HV0.5) using a Shimadzu HMV-2 microhardness tester. Measured values represent the average of five indentations together with the respective standard deviation as a measure for the error. Grain size has been measured by the lineal intercept method according to ASTM E112 [12]. Selected samples were further investigated with electron microscopy, including backscattered (BSD) and secondary electron (SE) imaging and energy-dispersive X-ray spectroscopy (EDS), for which a Leo 1550 FEG SEM equipped with an Oxford Instruments EDS detector has been used.

3 Results

3.1 Heat treatments

The microstructures obtained with the different heat treatments are shown in Fig. 1b–i together with the respective grain size

Fig. 2 a Sample design. b Disc with filled grooves. Note the restraint maximising stainless steel disc welded onto the bottom of the Haynes® 282® disc
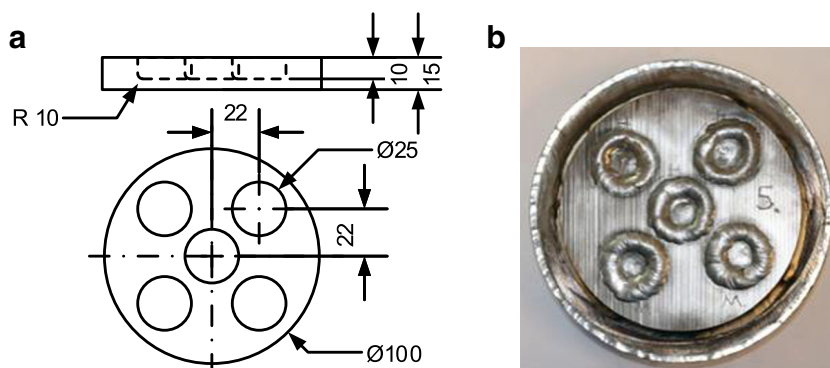
and hardness values. Grain size varied within one ASTM number for the different heat treatments, except for the discs heated to 1150 °C, which is above the secondary carbide solvus temperature. This led to significant grain growth, as indicated in Fig. 1e, i. The larger grain size did not have a measurable effect on the hardness. All age-hardened samples show hardness values between 370 and 380 HV. As expected, neither heat treatment was able to change the string-like carbide alignment present from the forging process (cf. Fig. 1). Based on the microstructural evaluation, the heat treatments of disc 1 (1010 °C 1 h) and disc 3 (1120 °C 0.5 h) show no striking difference, with the amount and distribution of carbides, while not quantified, appearing to be the same. The hardness values of the base material of discs 1 and 3 however were exceeding those being expected for precipitate-free material.

3.2 Repair welding

The general appearance of the repair-welded grooves is shown in Fig. 3, with the weld deposit layers being indicated by dashed lines. The groove's depth of 10 mm has been filled with seven to eight welding deposit layers, leading to an average layer thickness of 1.5 ± 0.3 mm. It has to be noted that the apparent layer thickness is lower than right after depositing, since some re-melting occurs during subsequent layer deposition. The welding deposits are further referred to as fusion zone, while the term heat-affected zone describes the
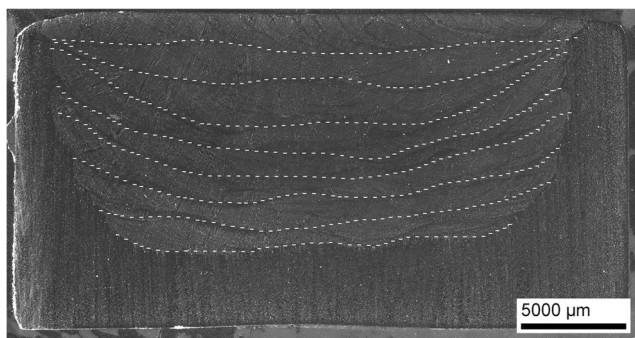

Fig. 3 Macro image of an etched cross section with several weld deposits visible in the fusion zone (as indicated by dashed lines)

heat-affected zone of the base material. The post weld heat-treated discs show a uniform hardness distribution over the whole weld area (120 A 402 ± 13 HV, 140 A 393 ± 15 HV), whereas a hardness drop below 300 HV is visible for the top fusion zone layers in the discs without PWHT, as visible in Fig. 4a. While this drop in hardness occurs in both welding conditions, the higher heat input of the samples welded with 140 A welding current led to a somewhat delayed but sharper reduction in hardness. The same hardness drop also occurs in the base metal HAZ, measurable on the side walls of the grooves, cf. Fig. 4b. The hardening response is however somewhat more rapid, since values below 300 HV were only measured adjacent to the 2 to 2.5 topmost layers.

3.3 Weld examination

No cracking has been observed in the heat-affected zone, irrespective of the pre and post weld heat treatment conditions. However, cracking was found in the fusion zone. As the base material condition did not show a measurable effect on the cracking behaviour in the fusion zone, the results were grouped based only on the heat input, further referred to as 140- and 120-A welding conditions. The metallographic examination of the weld fusion zone revealed a total of 23 cracks in the pre weld heat-treated discs (140 A 16; 120 A 7), while for the discs that have been put through a post weld heat treatment, a total number of 24 cracks was found (140 A 17; 120 A 7). Note that those numbers relate to the total number of grooves investigated. For comparison of the two welding conditions, the normalised number of cracks for the 140-A welding condition (10.67 and 11.33) should be used, since the sample ratio of 120-A and 140-A welding condition is 2:3 and hence the investigated cross section area is not the same (2 grooves 120 A vs. 3 grooves 140 A). The cracks run vertically along solidification grain boundaries and were hence classified as solidification cracks. No liquation cracks in the heat-affected zone between layers were found, while in total, 65 voids appear in these regions that show no signs of liquation. Initially believed to be strain age cracks, the voids appear to be Al-rich oxide inclusions, as will be discussed
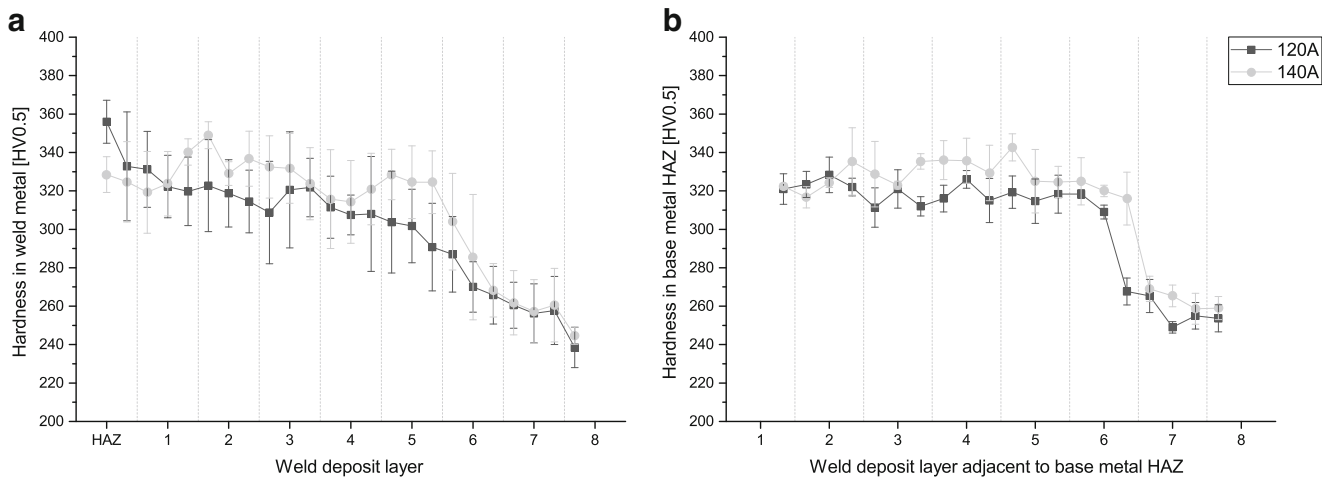
Fig. 4 Hardness evolution as a function of weld deposit layer for 120-A and 140-A welding current. **a** Weld metal. **b** Hardness in the base metal HAZ adjacent to the fusion zone. Indent spacing 0.5 mm

further. Lack of fusion has been observed in all samples, but was not further investigated. Solidification cracks had an average crack length of 375 μm, while LoF typically ranges from 500 to 1500 μm and the small voids around 100–200 μm. Figure 5 shows the total number of cracks per welding deposit layer for all pre and post weld heat-treated samples. Note that only solidification cracks are shown here, since these were the only cracks present in the material. While those cracks do not form during post weld heat treatment, the grouping of samples has been kept to point out that PWHT did not lead to more cracks in the material.

4 Discussion

The hardness of the heat-treated discs 1 and 3 is higher than one would expect for a precipitate-free material. Comparison with the as-received condition (cf. Fig. 1) and the finding that γ' precipitation is rather fast in Haynes® 282® [13] led to the conclusion that the forced convection cooling as used in this study still leads to significant hardening reactions in the material. The unexpected hardness difference between weld and base metal after post weld heat treatment could be related to a difference in size and volume fraction of the γ' phase, caused by the different thermal history. While present in the material, this difference did not affect the cracking response since both the solidification cracks and oxide inclusions remain from the welding process and were not caused by the post weld heat treatment.

No correlation could be found between thermal history of the base material and the cracking response. As cracks were only found in the weld fusion zone, this is however reasonable, as an effect of the base material could only be anticipated in FZ regions very close to the base material. The absence of
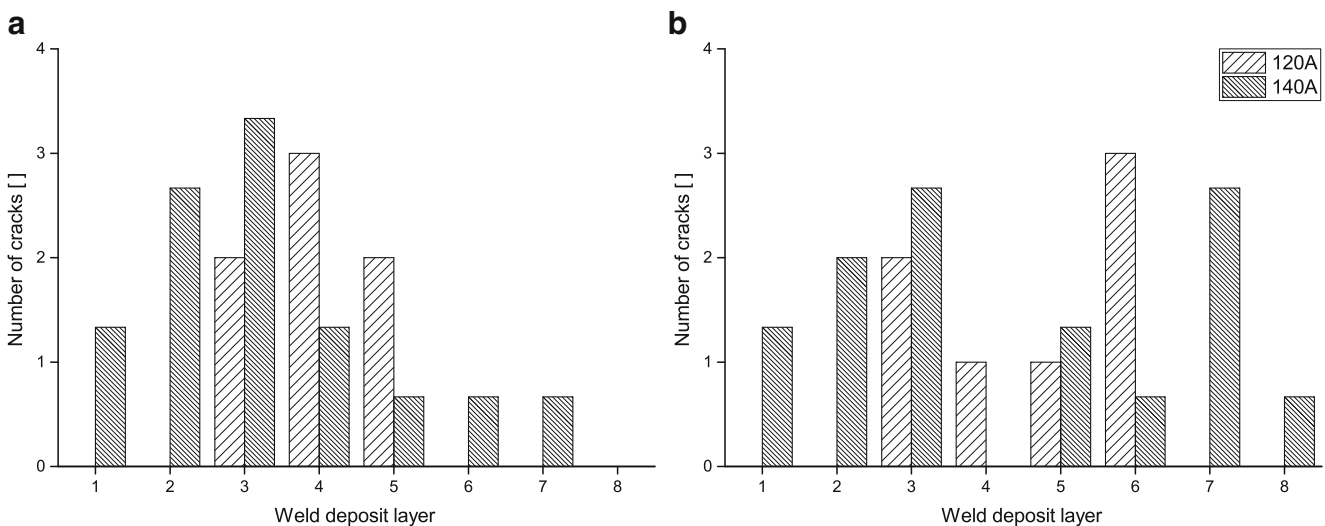

Fig. 5 Total number of cracks per weld deposit layer. **a** Pre weld heat-treated discs (1–4). **b** Pre + post weld heat-treated discs (5–8). Results for 140-A welding condition are normalised to account for the difference in sample size between the two conditions

cracks in the base metal HAZ would indicate that, irrespective of the material condition, wrought Haynes® 282® exhibits a generally good response to repair welding operations. This is however different for the fusion zone, where in total 47 cracks have been observed in the 40 investigated grooves. Welding with higher heat input increased cracking by a factor of 1.5, with no clear pattern being evident regarding overall crack distribution over the welding deposit layers. While stress levels have not been quantified within this study, it can be reasonably assumed that higher thermal stresses were present during welding with 140-A welding current and hence facilitating crack formation. SEM investigations of found cracks revealed the dendritic structure formed during the solidification process without signs of decohesion, as shown in Fig. 6. This further supports the assumption that those cracks are indeed solidification cracks.

The voids found in bottom regions of weld deposits appear to be cracks when viewed under an optical microscope, lying horizontally, i.e. parallel to the fusion boundary. Most of them are located at the interface between columnar grains on the bottom and equiaxed grains on top (cf. Fig. 7). No signs of liquation could be found during SEM investigation. EDS scans however revealed the presence of aluminium-rich oxide films in the voids, as indicated in Fig. 7. This finding makes it very unlikely that those voids are stain age cracks and instead support the hypothesis that these voids are caused by oxide films present during the deposition process. The large number in comparison to the amount of solidification cracks is related to the manual welding process, where more thorough surface cleaning between layer depositions would have been necessary. It should be noted though that voids caused by oxide layers are about half the size of solidification cracks and LoF (cf. Figs. 6 and 7).

The reduced hardness in the upper weld deposit layers indicates that three to four subsequently deposited layers are necessary to increase the hardness to above 300 HV.
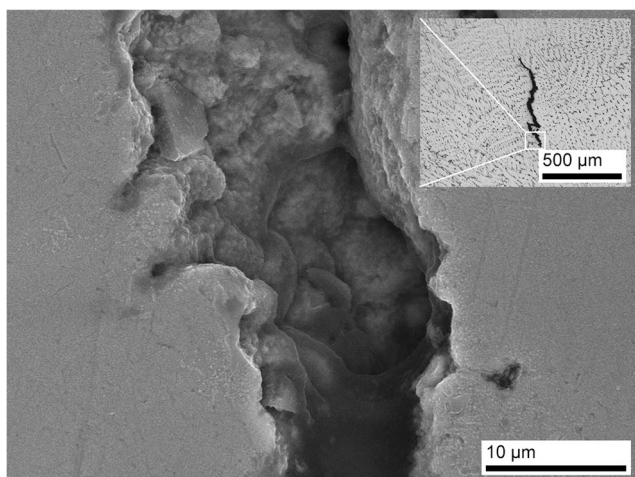
Fig. 6 Solidification crack in disc 8, 120-A welding condition. Clear indication of a dendrite structure in the crack opening. Crack length 706 μm
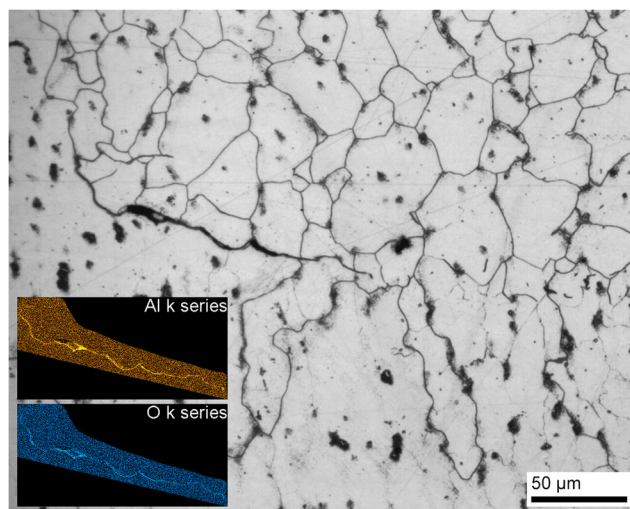
Fig. 7 Aluminium-rich oxide layer at a presumed layer start location in disc 6, 140-A welding condition. Note the equiaxed grain structure above the oxide layer. Void size 184 μm

Reaching values exceeding 300 HV already after two subsequent welding passes, the hardening response seems to be somewhat more rapid in the base metal HAZ. The absence of strain age cracks in all welds suggests that either the weld residual stresses were below a critical level or that the hardening response was too slow for strain age cracking to occur in the fusion zone material. Additional information is necessary to reveal more about the underlying mechanism, which could be achieved by experiments with controlled stress relaxation. This should enable a more reliable statement about the material susceptibility towards SAC.

5 Conclusions

The effect of multi-pass repair welding on wrought Haynes® 282® has been investigated. No cracking was found in the base material heat-affected zone, irrespective of base material microstructure, while cracking found in the fusion zone welding deposits has been identified as solidification cracking. Crack-like voids in bottom regions of weld deposit layers have been identified as aluminium-rich oxide layers not being removed between layer depositions. Higher welding current and hence increased heat input increased solidification cracking in fusion zone layers. Neither liquation cracking nor strain age cracking could be confirmed during this investigation.

References

1. Sims CT, Stoloff NS, Hagel WC (1987) Superalloys II. Wiley, New York

2. Andersson J (2011) Weldability of precipitation hardening superalloys: influence of microstructure. Doctoral Thesis, Chalmers University of Technology

3. Pike LM (2006) HAYNES® 282™ alloy—a new wrought superalloy designed for improved creep strength and fabricability. In: Proc. ASME Turbo Expo 2006 Power Land Sea air. ASME, Barcelona, pp 1031–1039

4. Sjöberg G (2010) Casting superalloys for structural applications. In: 7th Int. Symp. Superalloy 718 Deriv. The minerals, Metals & Materials Society, pp 117–130

5. Osoba LO, Ojo OA (2012) Influence of laser welding heat input on HAZ cracking in newly developed Haynes 282 superalloy. Mater Sci Technol 28:431–436. doi:10.1179/1743284711Y.0000000078

6. Andersson J, Sjöberg G, Chaturvedi M (2010) Hot ductility study of HAYNES 282 Ssperalloy. In: Proc. 7th Int. Symp. Superalloy 718 Deriv. The minerals, Metals & Materials Society, pp 539–554

7. Rowe MD (2006) Ranking the resistance of wrought superalloys to strain-age cracking. Weld J 85:27s–34s

8. Metzler DA (2008) A Gleeble®-based method for ranking the strain-age cracking susceptibility of Ni-based superalloys. Weld J 87:249s–256s

9. Osoba LO, Khan AK, Adeosun SO (2013) Cracking susceptibility after post-weld heat treatment in Haynes 282 nickel based superalloy. Acta Metall Sin Engl Lett 26:747–753. doi:10.1007/s40195-013-0252-3

10. Haynes International Inc. (2008) Haynes 282 Product Brochure

11. Prager M, Shira CS (1968) Welding of precipitation-hardening Nickel-base alloys. WRC Bulletin 128:1–55

12. ASTM E112-13 (2013) Standard test methods for determining average grain size. ASTM International, West Consohocken, PA

13. Denzler A, Gruber H, Henrikson J, Solbreck M (2012) Hårdhetsförändring vid Värmebehandling av Haynes® 282®. Bachelor Thesis, Chalmers University of Technology